STRUCTURALLY SIMPLE REDOX POLYMERSOMES FOR DOXORUBICIN DELIVERY

Elena Benito, Lucía Romero-Azogil, Elsa Galbis, M.-Violante de-Paz, M.-Gracia García-Martín

Departamento de Química Orgánica y Farmacéutica, Universidad de Sevilla, C/ Profesor García González 2, 41012 Sevilla, Spain.

Email: graciagm@us.es

ABSTRACT

A simple redox amphiphilic tri-block copolyurethane capable of assembling in the form of polymersome has been easily synthesized. Thus, the hydrophobic core is constituted by a central block containing multiple disulfide linkages, and the hydrophilic segments are formed by poly(ethylene glycol) methyl ether ($mPEG_{2000}$). The disulfide-containing block was obtained by the reaction of commercial 2,2'-dithiodiethanol and hexamethylene diisocyanate, which was further reacted with the mentioned PEG to afford the tri-block copolymer nominated as mPEG-PDH-mPEG, in above 80% yield. This copolymer self-assembled into polymersomes of size around 130 nm by the water addition/solvent evaporation method. Different systems of doxorubicin/polymer ratios (D/P 0.5 – 3) were prepared and the drug loading (%DL) and encapsulation efficiency (%EE) were studied by visible light absorbance measurements. Systems D/P 2 and 3 showed DL up to 62% and 69%, respectively. Besides that, D/P 1 and 2 presented EE values in the order of 83%. Finally, the release of DOX in the presence of 0.01 M glutathione solutions at 37 °C, was 74.6% and 82% from D/P 3 and D/P 0.5, respectively, after 5 days of incubation. Further studies on other water-soluble drugs for the cancer treatment would be of great interest to demonstrate the high potential of these redox polymeric systems.

Keywords

Stimuli-responsive polymersomes, copolyurethanes, redox-sensitive systems, doxorubicin, drug loading, drug delivery systems.

1. INTRODUCTION

Nowadays, cancer is one of the leading causes of mortality in developed countries and its incidence is increased every year [1]. The cancer treatment usually involves the administration of potent drugs to avoid both the spread and evolution of the disease to advanced stages. Nevertheless, the un-specificity of these agents against tumor cells, leads to low bioavailability, systemic toxicity, multidrug resistance, and other undesirable clinical effects [2,3]. In this sense an effective strategy to overcome limitations of chemotherapy is the use of drug-delivery systems (DDS), which prevent drug release in the bloodstream and healthy tissues, and specifically release the antitumor agent in the cancerous tissue [4,5]. Among the most appropriate materials for the manufacture of targeted drug delivery nanosystems are natural polymers (dextran, hyaluronic acid, chitosan, albumin, transferrin, and antibody) and synthetic polymers (PEG, polyesters, polycarbonates, polypeptides) together with liposomes [6]. Thus, stimuli-responsive liposomes, polymeric micelles, polymersomes (hollow vesicles), and hydrogels represent a breakthrough in personalized medicine for cancer diagnosis and therapy [7]. Furthermore, it has been demonstrated that these innovative DDS are able to specifically deliver nonselective drugs such as docetaxel, doxorubicin (DOX) hydrochloride, cisplatin, and mertansine [5].

Another key aspect in the development of biocompatible DDS [8,2] is they also improve the bioavailability of the encapsulated drug due to reduced interaction with plasmatic proteins, which increases the half-life of therapeutic agents and reduces the associated undesirable effects [9,10].

Among the most widely studied stimuli-response polymers are redox polymers, mostly those containing reducible disulfide bonds (S-S) either in the main chain as well as in the side chains [11]. The disulfide group is easily reduced to thiol groups (2 SH per S-S linkage) under hypoxic conditions such as the reduction conditions present in the tumor microenvironment. In view that the reductive glutathione (GSH) levels in tumor tissues is 4 times higher than those found in healthy tissues, many redox DDS containing disulfide groups have been synthesized and their efficiency studied [12-14].

In relation with the above mentioned DDS, polymersomes (PMS) are assembled from amphiphilic block-copolymers, and they are really interesting nanosystems as they present high stability, wide chemical versatility and they can incorporate both hydrophilic (within the aqueous core) and hydrophobic molecules (embedded in the membrane) [15]. In addition to this, depending on the copolymer composition and chain length the final sizes can be tuned to improve their membrane properties and stability [16,17].

Many researchers have focused their attention on the preparation of reduction-sensitive PMS for drug release in the tumor environment [10,18,19].

In order to improve the effectiveness of DDS for cancer treatment, sophisticated polymer structures have been synthesized but are economically more expensive and time-consuming [20-24]. Furthermore, to avoid premature leakage from DDS of encapsulated drugs through non-covalent interaction during blood circulation —which side effects cause toxicity— some authors have developed a strategy of covalently linking the drug to the polymeric system resulting in polymer prodrugs [14,25]. However, this strategy supposes more complex synthetic manufacturing processes.

Within the framework of our current research, a main objective is to develop a simple and reproducible methodology that allows us to obtain amphiphilic redox copolymers that are capable of self-assembling in the form of polymersomes, which can include hydrophilic drugs as HCl DOX in their aqueous core. We had already synthesized redox polymers containing disulfide bonds in the main chain and demonstrated their degradation by means of GSH [26-31].

In the present paper, we describe the synthesis and characterization of a simple linear amphiphilic tri-block copolymer along with the study of its ability to self-assemble into polymersomes. The copolymer was synthesized in two steps, we first prepared the hydrophobic central block containing multiple disulfide bonds, which was further extended with polyethylene glycol methyl ether (mPEG). PEG has been widely employed in DDS [10,32] since it is a safe-to-use material in humans, and it has been classified as Generally Regarded as Safe (GRAS) by the U.S. FDA [33].

Some advantages must be highlighted in relation with the easy accessibility to this polymer: it is obtained with high performance from commercial reagents through an easy and reproducible procedure, which can be easily scale-up for commercial purposes. Thus, the size and shape of the nanoparticles have been determined and Doxorubicin hydrochloride (HCl · DOX) was the selected drug to study their applicability in cancer therapy.

2. MATERIALS AND METHODS

2.1 Materials

Commercial reagents were purchased from Sigma-Aldrich Chemical Co. (Madrid, Spain) and used as received without further purification. Solvents of high purity grade were purchased from Merck (Darmstadt, Germany) and they were dried by appropriate standard procedures when necessary by the use of molecular sieves (Scharlab S.L., Sentmenat, Spain). Doxorubicin hydrochloride was purchased from LC Laboratories (Woburn, MA, USA).

2.2 General Methods

IR spectra were recorded on a Jasco FT/IR-4200 spectrometer (Easton, MD, USA) equipped with ATR. ^{1}H and ^{13}C NMR spectra were recorded at 300 or 353 K using a Bruker Advance AMX-500 (Francfort, Germany) at the *Centro de Investigación, Tecnología e Innovación* of the Universidad de Sevilla (CITIUS). Chemical shifts (δ) are reported as parts per million downfield from tetramethylsilane (Me_4Si). Two-dimensional shift correlation spectra, such as ^{1}H - ^{1}H homonuclear and ^{13}C-^{1}H heteronuclear were also recorded with the COSY and HETCOR pulse sequences, respectively. For the kinetic studies of the pre-polymer formation, the ^{1}H NMR and diffusion-filtered ^{1}H NMR spectra were recorded on a Bruker Avance III 500 MHz spectrometer equipped with a 5 mm TCI cryoprobe at 298 K, using triphenyl methane as a marker. Diffusion-filtered ^{1}H NMR spectra were carried out using the standard bipolar-gradient-pulse-pair longitudinal-eddy-current-delay (BPP-LED) pulse sequence [34]. A diffusion delay of 250 ms and bipolar pulsed gradient pairs of total duration 3 ms were used. The gradient amplitude was set to 95% of the maximum amplitude value. Accumulation of 32 scans was preceded by 4 dummy scans for each spectrum. Molecular weights were determined by size-exclusion chromatography (SEC) using Waters equipment (Milford, MA, USA) provided with a refractive-index detector 2414 (thermostated at 40 °C). *N,N*-dimethylformamide (DMF) containing LiBr (5.8 mM solution) was the mobile phase. Samples (100 µL of 0.1% (w/v) solution) were injected and chromatographed with a flow of 1 mL · min^{-1}. HR3 and HR4 Waters Styragel columns (7.8 × 300 mm) were used, linked in series and protected with a guard column, thermostated at 60 °C. Molar mass averages and their distributions were estimated against polystyrene standards. The thermal behavior of the copolymer was examined by differential scanning calorimetry (DSC) using a TA DSC Q200 Instrument (Milford, MA, USA) calibrated with indium. Samples of about 2–3 mg were heated at a rate of 10 °C · min^{-1} under a nitrogen flow of 50 mL · min^{-1}, and cooled to −35 °C. The melting temperature (T_m) was taken as the maximum of the endothermic peak appearing on heating traces recorded at 10 °C · min^{-1}, and the glass transition temperature (T_g) was taken as the temperature for the

inflection point seen on heating traces recorded at 20 °C · min^{-1} from samples quenched from the melt. Thermogravimetric analyses (TGA) were performed with a TA SDT Q600 thermobalance (Milford, MA, USA). Polymer samples, with a weight around 3–4 mg, were heated at a rate of 10 °C · min^{-1} within the temperature range of 30–600 °C under an inert atmosphere. The polymerization reaction assays were performed in the absence of humidity, under an inert atmosphere. All glassware was heated overnight at 80 °C before use. The pure monomers were dried under vacuum and stored under an inert atmosphere until required.

The average diameter and size distribution of the samples were determined with a Malvern Zetasizer Nano ZS (Malvern Instruments, Malvern, UK) at 25 °C with a particle size analysis range of 0.6 nm to 6 μm by Dynamic Light Scattering (DLS) and the results are given as volume distribution of the major population by the mean diameter with its standard deviation. The morphology and distribution of the nanoparticles were characterized by Scanning Electron Microscopy (SEM) using a field emission HITACHI S5200 microscope operating at 5 kV and by Transmission Electron Microscopy (TEM) using a ZEISS Libra-120 transmission electron microscope operating at 80 kV at the CITIUS Service (University of Seville). The best images in SEM analysis were obtained when the dispersions were deposited and allowed to dry for 24 h on a platinum support before covering them with platinum. Fluorescent images were obtained with a STED Abberior Facility Line equipment (Abberior Instruments, Göttingen, Germany) at an excitation wavelength of 561 nm. Visible light absorbance measurements were conducted on an Agilent 8453 UV-Visible spectrophotometer (Palo Alto, USA), equipped with diode array detection (DAD). Each data was obtained from, at least, three measurements.

2.3 Synthetic procedures and nanoparticle formation

2.3.1 Kinetic study on the formation of hydrophobic block PDH

A kinetic study on the formation of the hydrophobic segment PDH was carried out by ^{1}H NMR. Thus, a dry NMR tube was loaded with 2,2'-dithiodiethanol (DiT) (55 mg, 0.356 mmol), hexamethylene diisocyanate (HMDI) (0.06 mL, 0.374 mmol, 5% excess) and deuterated DMSO-d_6 (0.7 mL) under inert atmosphere. Triphenyl methane (10.4 mg, 0.042 mmol) was also added as a marker. The final monomer concentration in the mixture was 6.8 % w/v and 7.8 % w/v for DiT and HMDI, respectively. All ^{1}H NMR spectra were recorded at 25 °C, over 3 hours, at regular intervals of 30 min. A first spectrum was registered before the addition of the catalyst [dibutyltin (II) dilaurate] (0.2%-mole relative to the monomers). Then, the reaction proceeded into the NMR rotor, and the extent of the reaction was followed by ^{1}H NMR and diffusion-filtered ^{1}H NMR, as above mentioned (Figure 1). NMR data of the diisocyanate PDH intermediate are given next.

^{1}H NMR (DMSO-d_6, 500 MHz): δ (ppm) 1.19-1.30 (m, n·4H, -C*H*$_2$CH$_2$CH$_2$NH and -C*H*$_2$CH$_2$CH$_2$NCO), 1.31-1.45 (m, n·4H, -CH$_2$C*H*$_2$CH$_2$NH and CH$_2$C*H*$_2$CH$_2$NCO), 2.82 (t, 2H, *J* = 6.43 Hz, SC*H*$_2$CH$_2$OH), 2.90-3.03 (m, n·8H, -CH$_2$CH$_2$C*H*$_2$NH and SC*H*$_2$CH$_2$O), 3.64 (t, 2H, *J* = 6.25 Hz, SCH$_2$C*H*$_2$OH) 4.18 (t, n·4H, *J* = 6.17 Hz, SCH$_2$C*H*$_2$O), 5.72 (bs, NH urea), 6.18, 7.13 (2 bs, NH).

^{13}C NMR (DMSO-d_6, 125 MHz): δ (ppm) 26.4, 26.5, 26.6 (-*C*H$_2$CH$_2$CH$_2$NH and *C*H$_2$CH$_2$CH$_2$NCO), 29.8 (-CH$_2$*C*H$_2$CH$_2$NH), 30.5 (-CH$_2$*C*H$_2$CH$_2$NCO), 37.7 (S*C*H$_2$CH$_2$O), 40.4 (-CH$_2$CH$_2$*C*H$_2$NH), 41.7 (S*C*H$_2$CH$_2$OH), 59.9, 60.1 (SCH$_2$*C*H$_2$OH), 62.1, 62.2 (SCH$_2$*C*H$_2$O), 155.9, 156.4 (CO urethane), 158.6 (CO urea).

2.3.2 Synthesis and characterization of tri-*block* polyurethane mPEG-PDH-mPEG

A round-bottom flask was loaded with 2,2'-dithiodiethanol (DiT) (0.245 mL, 2 mmol) and the system was treated with three cycles of vacuum-argon before the addition of dry *N,N*-dimethylacetamide (DMA) (4 mL). The mixture was stirred to get an homogeneous solution and then hexamethylene diisocyanate (HMDI) (0.340 mL, 2.1 mmol, 5% excess) was added under an argon atmosphere, followed by the catalyst [dibutyltin (II) dilaurate] (0.2%-mole relative to the monomers). Thus, the monomer concentration was fixed at 7.76 % w/v and 6.74 % w/v for HMDI and DiT, respectively. After stirring at room temperature for 2 hours, a solution of 2000 g · mol^{-1} poly(ethylene glycol) methyl ether ($mPEG_{2000}$) (195 mg, 0.097 mmol) in DMA (1 mL) was added. Stirring was continued at room temperature for 24 hours. Finally, the reaction mixture was diluted with chloroform (5 mL) and added dropwise into cold diethyl ether (400 mL). The precipitated polymer was filtered, washed with diethyl ether and dried under vacuum at 40 °C for 24 h. The mPEG-PDH-mPEG copolyurethane was isolated as a white solid (704 mg, 82%).

SEC data: M_w 25804; M_n 25164; M_w/M_n 1.02. IR: ν (cm^{-1}) 3321 (N-H), 2858 (O-C), 1677 (C=O urethane), 1530 (N-H urethane), 1261 (N-CO-O).

^{1}H NMR (DMSO-d_6, 500 MHz): δ (ppm) 1.21-1.32 (m, n·4H, -C*H*$_2$CH$_2$CH$_2$NH), 1.35-1.47 (m, n·4H, -CH$_2$C*H*$_2$CH$_2$NH]), 2.90-3.03 (m, n·8H, -CH$_2$CH$_2$C*H*$_2$NH and SCH$_2$), 3.27 (s, 6H, CH$_3$), 3.48-3.59 (m, 352H, OC*H*$_2$C*H*$_2$O), 4.19 (t, n·4H, J = 6.27 Hz, SCH$_2$C*H*$_2$O), 5.54 (bs, NH urea), 6.80 (bs, n·2H, NH).

^{13}C NMR (DMSO-d_6, 125 MHz): δ (ppm) 25.5 (-*C*H$_2$CH$_2$CH$_2$NH), 28.9 (-CH$_2$*C*H$_2$CH$_2$NH), 37.3 (S*C*H$_2$CH$_2$O), 40.4 (-CH$_2$CH$_2$*C*H$_2$NH), 57.7 (OCH$_3$), 61.4 (SCH$_2$*C*H$_2$O), 69.5 (O*C*H$_2$*C*H$_2$O), 71.3, 72.3 (*C*H$_2$OCH$_3$), 155.4 (CO).

TGA data: T_d: 259 °C (Decomposition temperature associated to 10% weight loss) and T_{ds}: 264 and 340 °C (Maximum decomposition temperature associated to 92% weight loss).

DSC data: T_m: 145 °C; ΔH_m: 51 J · g^{-1} (Melting enthalpy); T_g: 1 °C.

2.4 Formation of nanoparticles through self-assembly process

The nanoparticles were prepared following the method described by [35]. The tri-block copolymer mPEG-PDH-mPEG (100 mg) was dissolved in THF (10 mL) at room temperature with vigorous stirring under inert atmosphere. Then Milli-Q water (20 mL) was added dropwise at a rate of 0.1 mL · h^{-1} for 9 days. Then, the flask remained open for 48 hours to allow a slow evaporation of the solvent. The final micellar dispersion obtained had a polymer concentration of 5 mg · mL^{-1}.

2.4.1 Determination of the critical micelle concentration (CMC)

The CMC was determined by visible spectroscopy (at 600 nm) according to the method previously described by our research group [36]. The visible light absorbance of ten polymer solutions, with concentrations between 0.5 and 0.0074 mg · mL^{-1}, were measured by triplicate, at 600 nm using distilled water as a blank. The obtained data were plotted as a function of the polymer concentration and the CMC was established as the intersection between the straight trend lines at the lower and the upper concentrations.

2.5 Drug Loading and release

2.5.1 Loading of Doxorubicin into nanoparticles

Kinetics studies of the ability of nanoparticles to load an antitumor agent such as doxorubicin were carried out as follows: 5 mL of an aqueous solution of doxorubicin at different concentrations (0.125, 0.25, 0.5 and 0.75 mg · mL^{-1}) were placed into a falcon tube with a stirring bar; then 5 mL of the micellar dispersion with a concentration of 0.25 mg · mL^{-1} was placed into a mini-dialysis tube (1 kDa cut-off, GE Healthcare, Pittsburgh, PA, USA), previously soaked in water for 12 hours, and immersed in the falcon tube. Final polymer concentration was 0.125 mg · mL^{-1} in all cases and final drug concentration

was 0.0625, 0.125, 0.25 and 0.375, with a drug/polymer ratio of 0.5, 1, 2 and 3, respectively (D/P 0.5, D/P 1, D/P 2 and D/P 3 systems, respectively). The systems were stirred at 37 °C and the absorbance of the drug solutions measured at the maximum absorption of doxorubicin: 480 nm, at predetermined intervals from time = 1 hour to time = 7 days. Distilled water was used as a blank in each trial.

The concentration of DOX in the medium was determined by UV spectroscopy. Prior to the analysis, calibration was made with doxorubicin aqueous solutions (20-100 $\mu g \cdot mL^{-1}$) at 480 nm (See SI, Figure S1).

Drug loading (DL) and encapsulation efficiency (EE) of the DOX incorporated in the polymersomes were calculated according to equations (1) and (2).

$$DL = \frac{\textit{mass of DOX loaded into PMS}}{\textit{total mass of DOX-loaded PMS}} \; x\,100 \qquad (1)$$

$$EE = \frac{\textit{mass of DOX loaded into PMS}}{\textit{mass of DOX loaded at } t_0 \textit{ in the incubation tube}} \; x\,100 \qquad (2)$$

2.5.2 Release of DOX from glutathione-sensitive nanoparticles

2 mL of each DOX-loaded nanoparticle solutions were placed into a mini-dialysis tube and immersed in a falcon tube containing 9 mL of a glutathione (GSH) solution (0.01 M) and a stirring bar. The system was stirred at 37 °C and 5 mL of the external solution were replaced with 5 mL of fresh GSH solution at predetermined intervals. The release profiles were determined by measuring the absorbance at 480 nm of the external solution at intervals from 1 hour to 9 days. Thus, the released amount of DOX into such solutions was determined in relation with the calibration curve (Section 2.4.1). A freshly prepared GSH solution was used as a blank in each trial.

3. RESULTS AND DISCUSSION

3.1 Preparation of tri-block copolymer-based nanoparticles

3.1.1 Synthesis and chemical structure of amphiphilic tri-block copolyurethane mPEG-PDH-mPEG

The synthesis of the tri-block copolymer mPEG-PDH-mPEG was carried out from DiT, HMDI and $mPEG_{2000}$, in *N,N*-dimethylacetamide at room temperature, as it is shown in Scheme 1.

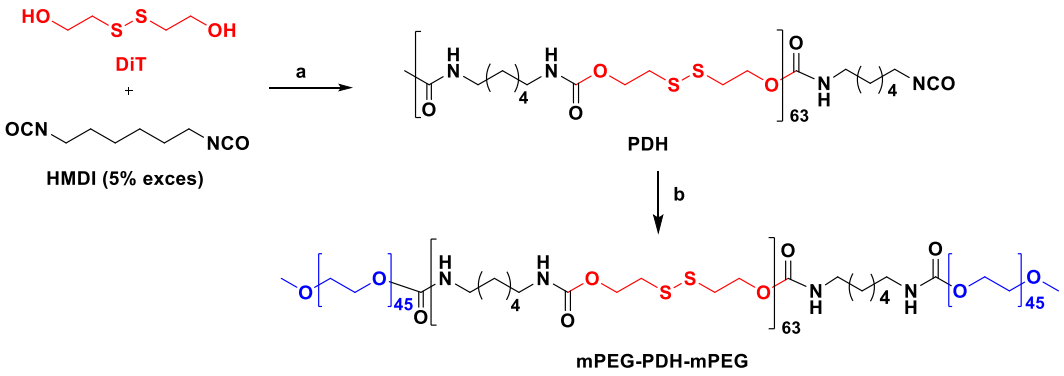

Scheme 1. Synthesis of mPEG-PDH-mPEG. a) Dry *N,N*-dimethylacetamide, dibutyltin (II) dilaurate, r. t.,b) *N,N*-dimethylacetamide, $mPEG_{2000}$, r. t.

Firstly, the formation of the disulfide-containing PDH block was followed by a kinetic study through ^{1}H NMR in dry DMSO-d_6, at 30-minute intervals for 3 h (Figure 1). The molar ratio for DiT-HMDI was fixed at 1:1.05, with initial concentration of DiT 0.44 M, and HMDI 0.46 M. Then, the amount of catalyst [dibutyltin (II) dilaurate] was fixed at 0.2%-mole relative to the monomers. All spectra were recorded as described in Section 2.3.1. The conversion (%) of the reaction was calculated by comparison of the integration of the signals at δ 3.64 ppm and δ 4.18 ppm corresponding to protons SCH_2CH_2OH of the DiT monomer (signal f in Figure 1), and those that correspondingly were incorporated in

the PDH block (SCH_2CH_2O), respectively. The singlet at δ 5.61 ppm due to the methyne group (CH) of triphenyl methane (marker) was used as the reference for such integrations.

The signal at δ 5.54 ppm indicated the presence of the formation of certain amount of urea groups. This can be due to the hydrolysis of the isocyanate function either of the HMDI monomer or the terminal groups of the PDH block owed to the hygroscopic nature of the mixture. So that, small amount (11%) of terminal S-S-CH_2CH_2OH groups corresponding to the PDH block (signals f' and g') could be observed (Figure 2).

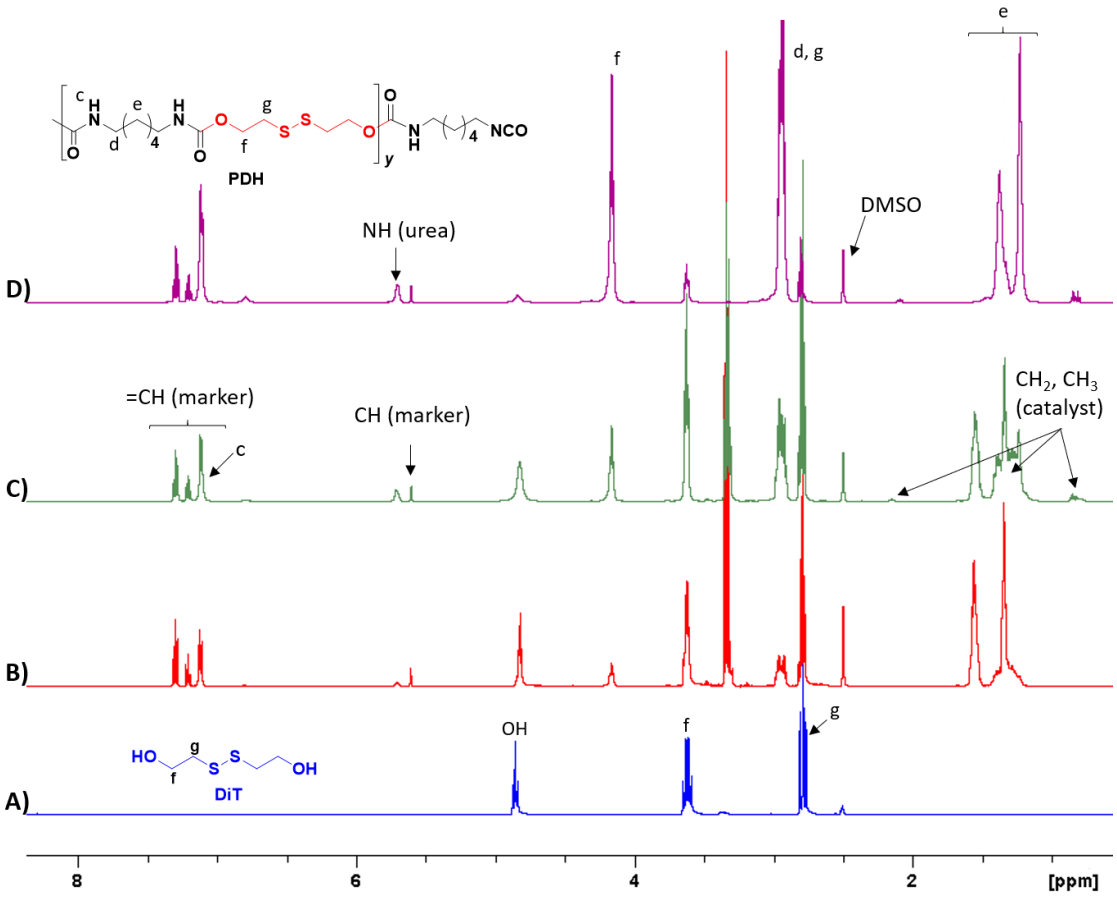

Figure 1. Polymerization progress for the synthesis of the PDH block by dry ^{1}H NMR in DMSO-d_6 at 298 K. A) Dithiodiethanol monomer as reference; Reaction mixture after B) 5 min; C) 35 min; D) 125 minutes.

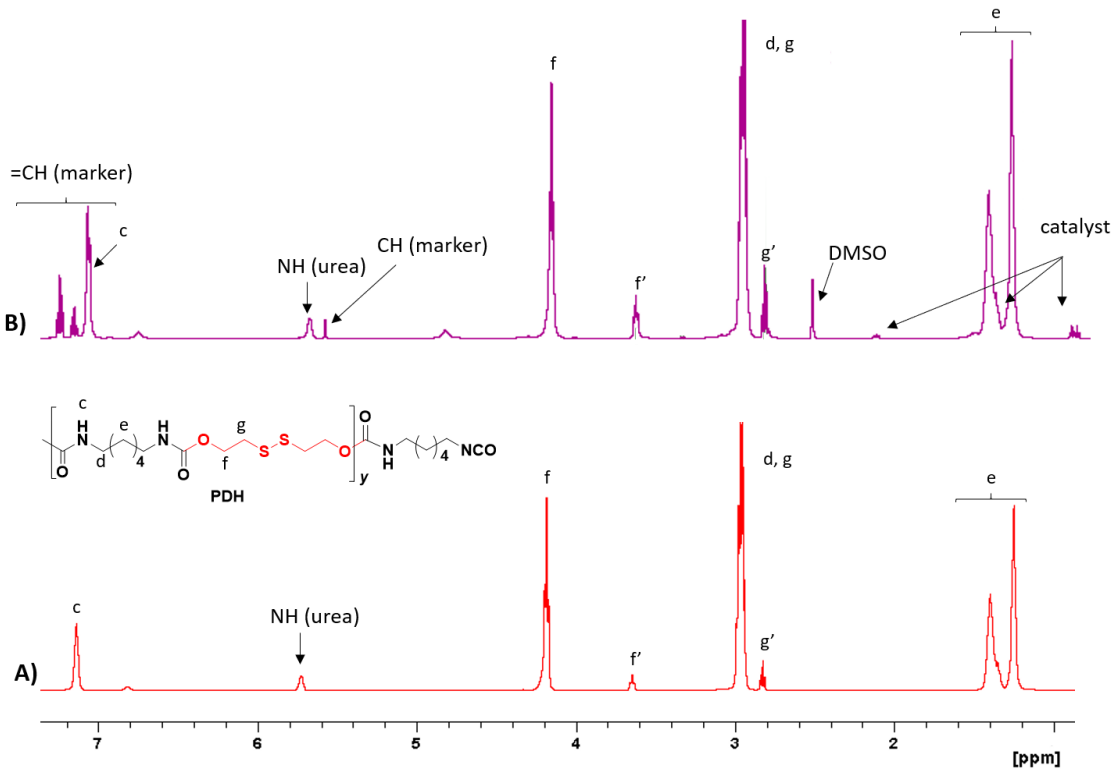

Figure 2. A) Diffusion-filtered ^{1}H NMR spectrum and B) ^{1}H NMR spectrum of diisocyanate PDH block, respectively, after 125 minutes.

The conversion was plotted versus time (Figure 3A), showing a conversion of 85.9% after 2 h. Figure 3B shows plots of the concentration of unreacted hydroxyl groups of dithiodiethanol at time *t* (1/[DiT]) versus time. Linear least-square analysis gives a value of 0.98 for R^2 for the first-order plot, suggesting a second-order kinetics mechanism for this reaction.

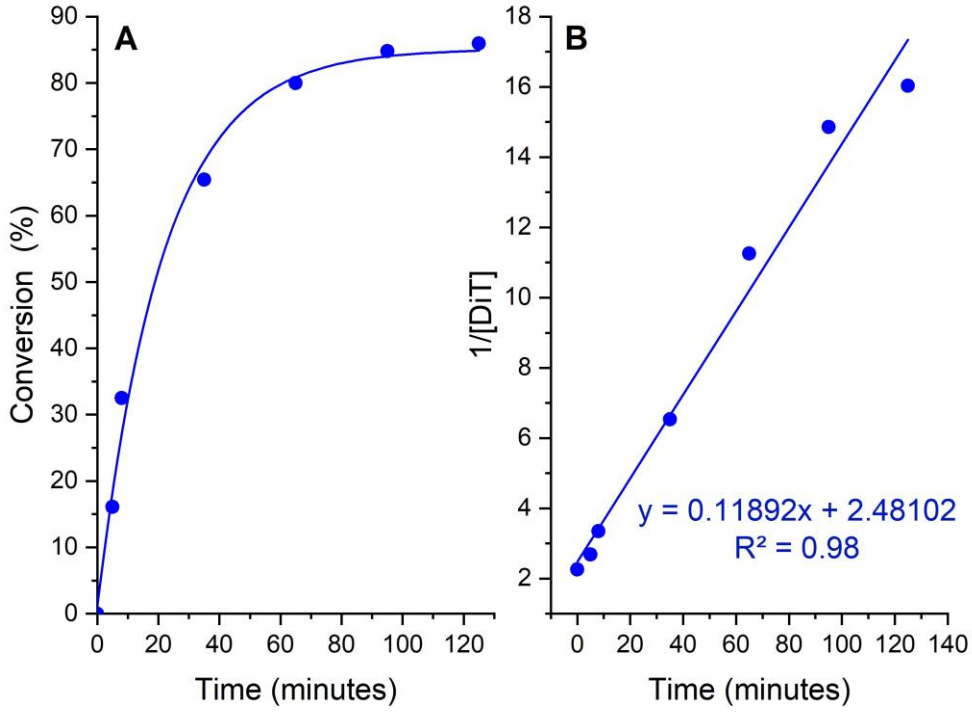

Figure 3. A) Conversion vs. time plot and B) 1/[dithiodiethanol] vs. time plot for the PDH block formation after 2 h.

For the synthesis of mPEG-PDH-mPEG (Scheme 1), the hydrophobic segment PDH was obtained from of 2,2'-dithiodiethanol (DiT) and 5% excess of hexamethylene diisiocyanate (HMDI) at room temperature, under inert atmosphere, using dry *N,N*-dimethylacetamide as solvent and dibutyltin (II) dilaurate as catalyst. SEC of PDH showed M_w 28500 g · mol^{-1} and low dispersity value of 1.05. (See SI, Figure S2). This low dispersity found was not expected according to the step-growth polymerization synthesis. This fact could be due to some fractionation process during the isolation of the sample. In addition, the SEC system employed using polystyrene standards could influence the final results as we have already observed in other investigations [37]. Subsequently, mPEGylation of the diisocyanate PDH intermediate was carried out by the addition of methyl ether PEG ($mPEG_{2000}$) in the calculated amount (0.097 mmol). The tri-block copolymer mPEG-PDH-mPEG was isolated in 82% yield, and was characterized by SEC, FTIR and NMR spectroscopies, and thermal analysis. The weight-average

molecular weight M_w was 25800 g · mol^{-1}, with a low dispersity value of 1.02 (See SI, Figure S3), which was in agreement with the molecular size of the PDH block. The apparent bimodal distribution in SEC chromatogram could be due to the chain extension of block PDH by mPEG$_{2000}$ to obtain the tri-block copolymer [38].

The corresponding FTIR-ATR and ^{1}H NMR and ^{13}C NMR spectroscopic data are detailed in section 2.3.2. The IR spectra showed the characteristic absorption bands of the urethane group at the predicted positions ν (cm^{-1}) 1677 (C=O urethane), 1530 (N-H urethane) [26] (See SI, Figure S4).

Likewise, the ^{1}H NMR spectra showed the expected signals corresponding to both PDH block and the hydrophilic blocks based on mPEG (Figure 4). By integration of the ^{1}H NMR signals at δ 3.27 ppm (CH_3) and δ 4.19 ppm (SCH_2CH_2O) (and simple proportion calculations, we determined the formation of the central segment with n = 63 and two terminal mPEG, which corresponds to a number-average molecular weight M_n of 24286 g · mol^{-1} (See SI, Figure S5). ^{1}H NMR spectra also showed a signal at δ 5.54 ppm due to some urea groups formation that was estimated in 3.6%. The reason may be the absorption of moisture by the highly hydrophilic PEG blocks, which can cause hydrolysis of the isocyanate function of the HMDI monomer or the PDH block end groups. In the ^{13}C NMR spectra of mPEG-PDH-mPEG only one signal at δ 155.4 ppm of the urethane carbonyl group was detected.

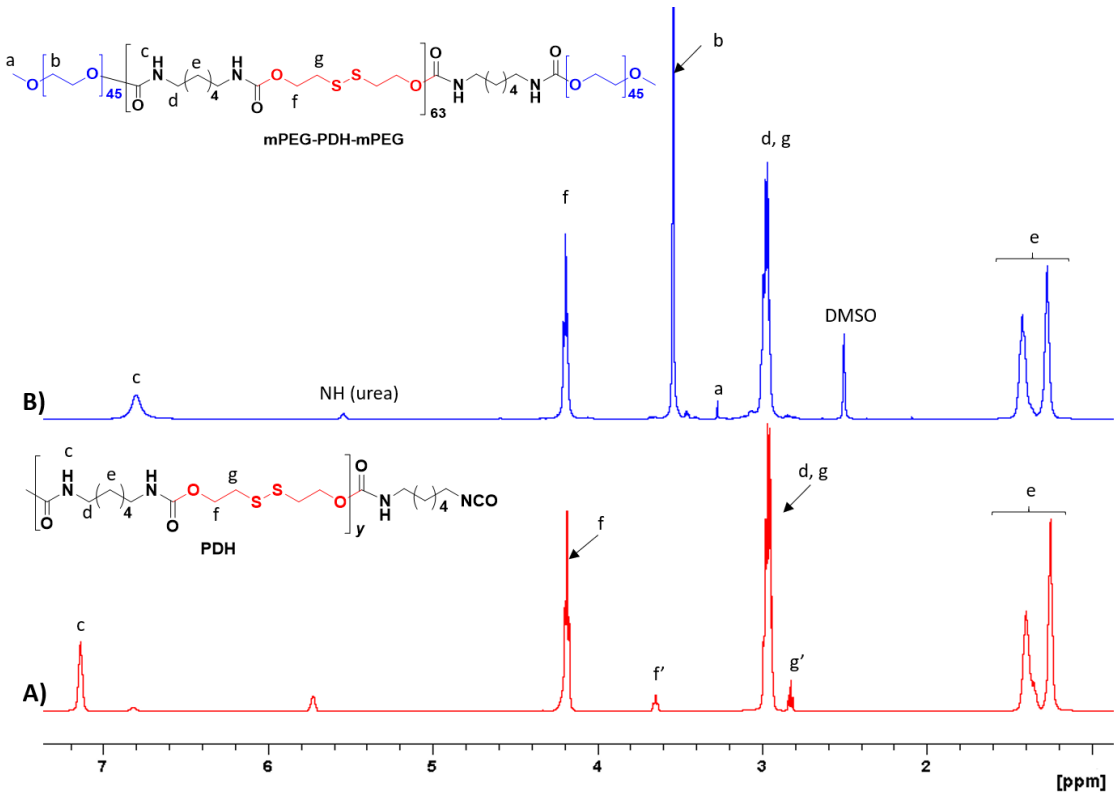

Figure 4. A) Diffusion-filtered ^{1}H NMR spectrum of diisocyanate PDH block; B) ^{1}H NMR spectrum of mPEG-PDH-mPEG.

The thermal properties of the synthesized polymer were studied by TGA and DSC (Table 1). TGA studies showed that the copolymer is stable to thermal degradation under inert atmosphere up to 250 °C with a decomposition onset temperature associated to 10% weight loss around 260 °C. Its degradation proceeded in two stage with maximum decomposition temperatures at 264 and 340 °C, with a total associated weight loss about 92%. This indicates that this material shows high thermal stability (Figure 5). On the other hand, the DSC studies showed that mPEG-PDH-mPEG was semicrystalline with T_m 145 °C and a melting enthalpy of 51 J · g^{-1} at the first heating. The second heating showed T_g at 1 °C.

By comparison reasons, thermal properties of commercial starting mPEG were also determined. TGA analysis showed that mPEG is stable above 340 °C and presented a degradation in one single stage with maximum decomposition temperature at 386 °C, with 98% weight loss associated (See SI, Figure S6). The degradation pattern observed

for the three-block copolymer was very similar to that of the PDH block that we had previously described [26]. Thus, PDH and mPEG-PDH-mPEG showed three and two degradation steps, respectively. They both showed maximum decomposition temperatures due to disulfide bonds degradation at 268 ºC and 264 ºC, respectively, as it can be seen in Table 1. This main degradation may involve the cleavage of the disulfide bond by β-elimination and the formation of elemental sulfur and terminal alkenes.

DSC analysis showed that mPEG had lower melting temperature than the tri-block polymer, with a value of 56 °C and a melting enthalpy of 194 $J \cdot g^{-1}$ at the first heating (See SI, Figure S7). mPEG also showed a crystallization transition in the cooling cycle at 35 °C with an associated enthalpy of 174 $J \cdot g^{-1}$. No T_g was observed for commercial mPEG but similar T_g was found for both PDH and tri-block copolymer.

Table 1. Thermal properties of commercial $mPEG_{2000}$, PDH and mPEG-PDH-mPEG.

Polymer	**TGA**			**DSC**				
	T_d[a] (°C)	T_{ds}[b] (°C)	ΔW[c] (%)	T_g[d] (°C)	T_m[e] (°C)	ΔH_m[e] (J/g)	T_c[f] (°C)	ΔH_c[f] (J/g)
Commercial mPEG	352	386	98	-	56	194	35	174
PDH[g]	266	**268**/359/450	**67**/18/11	1	147	63	105	-44
mPEG-PDH-mPEG	259	**264**/340	**67**/26	1	145	51	-	-

[a] Temperature at which 10% weight loss was observed in the TGA traces recorded at 10 °C · min^{-1}. [b] Decomposition temperatures measured at the peaks of the derivative curves; major peaks due to decomposition of disulfide bonds in bold. [c] Loss weight at the end of the decomposition step. [d] Glass transition temperature taken as the inflection point of the heating DSC traces of melt-quenched samples recorded at 20 °C · min^{-1}. [e] Melting temperature (T_m) and respective enthalpy (ΔH_m) measured by DSC at heating rates of 10 °C · min^{-1}. [f] Crystallization temperature (T_c) and respective enthalpy (ΔH_c) measured by DSC at heating rates of 10 °C · min^{-1}. [g] Reference [26].

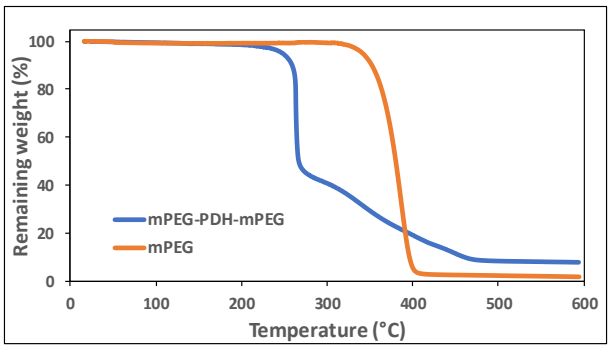

Figure 5. Comparative curves of thermal degradation under inert atmosphere of mPEG-PDH-mPEG and commercial mPEG. Remaining weight (%) vs. temperature.

3.1.2 Nanoparticle formation and characterization

The self-assembly ability of the mPEG-PDH-mPEG to form polymersomes in aqueous media and the critical micelle concentration (CMC) have been studied. The polymersomes were obtained by the water addition/solvent evaporation method, through slow addition of water to a polymer solution in THF, as described in Section 2.4. After evaporating the organic solvent, the aqueous phase was analyzed by dynamic light scattering (DLS) to determinate the diameter and size distribution of the formed vesicles. These experiments showed that a dispersion of almost monodispersed nanoparticles was achieved at a polymer concentration of 5 mg · mL^{-1} (PDI = 0.11) with hydrodynamic diameter around 130 nm (Figure 6A). Such samples were re-analyzed by DLS after 3 and 5 months, and no changes in particle size and PDI were observed with respect to initial measurements.

The aqueous phase was also studied by Transmission Electronic Microscopy (TEM) and Scanning Electronic Microscopy (SEM). Micrographs attained by TEM and SEM are shown in Figure 6B and 6C, respectively. SEM´s micrographs show spherical particles with sizes in the interval 125-180 nm, and aggregates with sizes over 1 μm can also be

observed. The formation of such aggregates may be due to the application of high vacuum entailed by the technique itself.

The results obtained by the three techniques were convergent, that is, similarities were observed from the data obtained.

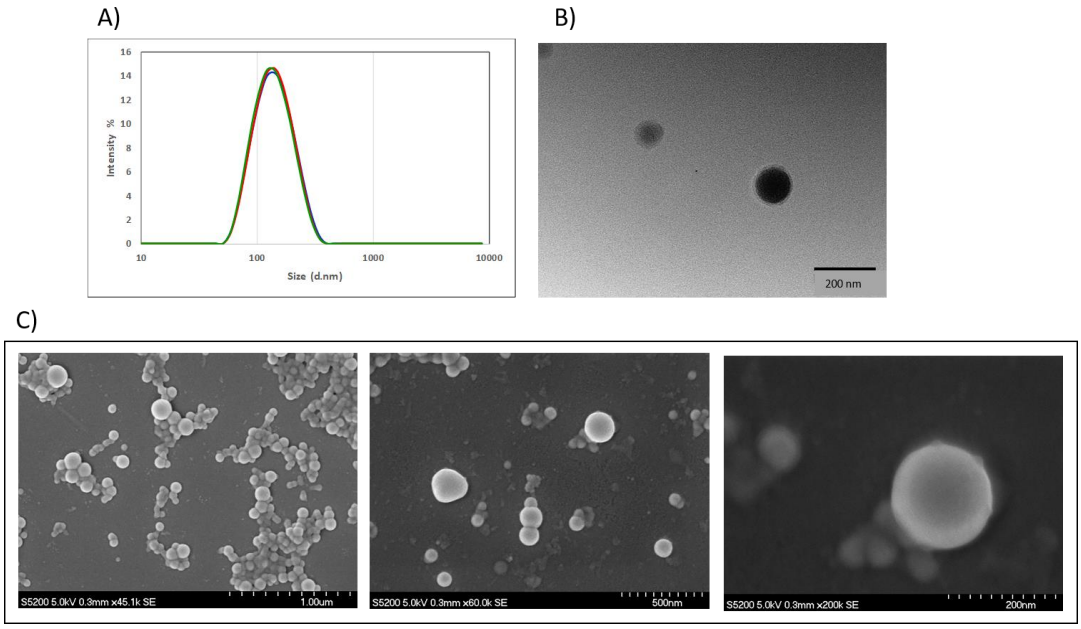

Figure 6. Characterization of polymersomes from mPEG-PDH-mPEG by DLS and Microscopy. A) Size distribution intensity graphs by DLS; B) TEM micrographs; C) SEM micrographs.

3.1.3 Critical Micelle concentration (CMC)

The CMC was calculated by visible spectroscopy. The absorbances of ten aqueous solutions of the nanoparticle dispersions were measured at 600 nm and the obtained data were plotted against polymer concentration. The plot showed that polymer solutions with concentration below 0.03 mg · mL^{-1} did not exhibit a marked absorbance. However, at higher concentrations, higher than 0.1 mg · mL^{-1}, a change in trend was observed, and the absorbance of the dispersions significantly increased in line with the concentration (Figure 7). In addition, samples with the highest concentrations showed a bluish hue, which is typical in micellar dispersions. The CMC was obtained from the cutoff

point of the straight lines obtained from the analysis of the trends of the nanoparticle solutions at low and high concentrations, resulting in a CMC value of 0.038 mg · mL^{-1}. This result highlights the great self-assembly tendency of the synthesized tri-*block* copolymer at very low polymer concentration.

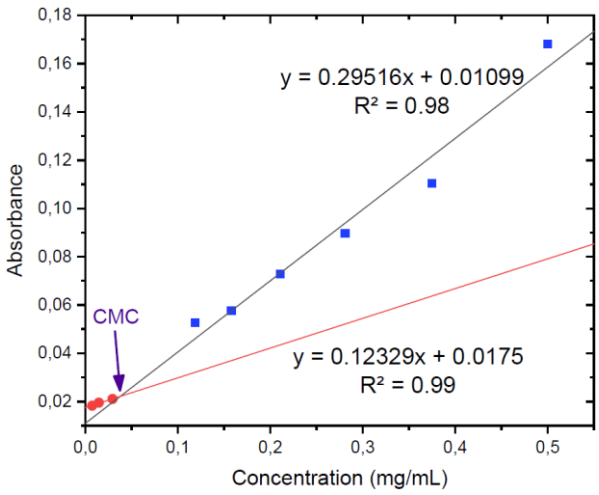

Figure 7. Absorbance of aqueous copolymer solution at a wavelength of 600 nm against polymer concentration.

3.2 Drug Loading

3.2.1 Loading of DOX

Doxorubicin is an effective antitumor drug for the treatment of certain cancers, such as some type of leukemia, Hodgkin's lymphoma, as well as breast cancer, gallbladder cancer or head and neck cancer [39-41]. For the drug loading, the polymersome dispersions were put in contact with a solution of DOX at drug/polymer ratios of 0.5, 1, 2 and 3 (named as D/P 0.5, D/P 1, D/P 2 and D/P 3, respectively), at 37 °C through a membrane. The incorporation of DOX into the polymersomes was assessed by determining the amount of drug remaining in the external solution through Visible Spectroscopy, because DOX shows a characteristic absorbance peak at 480 nm. DOX was quickly loaded within the first 10 hours and needed 50 hours to become stabilized.

The encapsulation efficiencies [EE (%)] for the four systems were found to be in the range 74 – 84% (Figure 8A). The evolution of EE was equivalent for the three designed trials with the lowest drug/polymer ratios, whereas the cumulative values of EE decreased when the DOX concentration was the highest used, which could be due to the saturation of the nanosystem. Conversely, as can be seen in Figure 8B, the drug loading [DL (%)] experienced a progressive increase, as did the drug/polymer ratio, which is seen in the range 29 – 69%. These values are indicative of excellent DOX uptake capacity. We had stated that one of the main parameters with a weight influence on drug loading and encapsulation efficiency of camptothecin into polymer nanoparticles is the drug/polymer ratio in the feed [42 and references therein]. In general terms, it was observed that the bigger the drug concentration in the feed, the higher was its EE. This is especially accurate as long as the drug was soluble in the media.

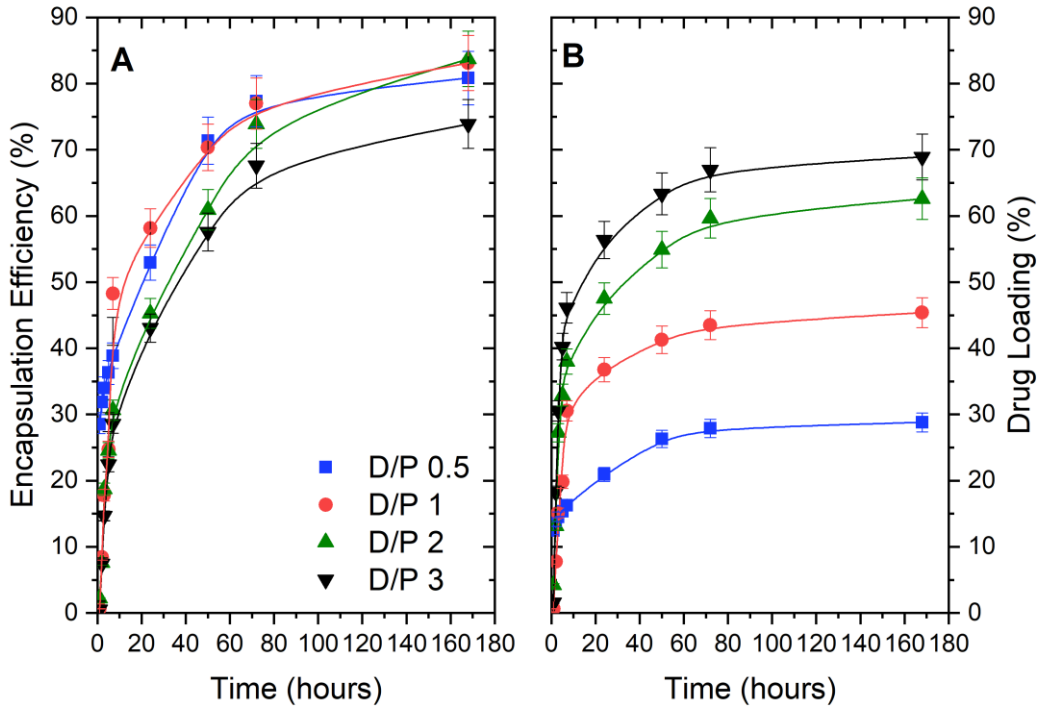

Figure 8. Drug loadings and encapsulation efficiencies of DOX/mPEG-PDH-mPEG systems (ratio D/P). A) DOX Encapsulation efficiency at drug/polymer ratios D/P 0.5, D/P 1, D/P 2 and D/P 3, respectively; B) Final drug loading percentage for the same ratios. Standard deviations are plotted with error bars in the graphs.

The loaded nanoparticles were analyzed by DLS, SEM and Fluorescence microscopy. The DLS results showed that after loading the drug the particle size increased in percentages from 23 to 114% (Figure 9) depending on the system. This effect has been observed by different authors, for instance in the case of bovine serum albumin–poly(L-lactic acid)-based nanoparticles for anticancer drug delivery [43].

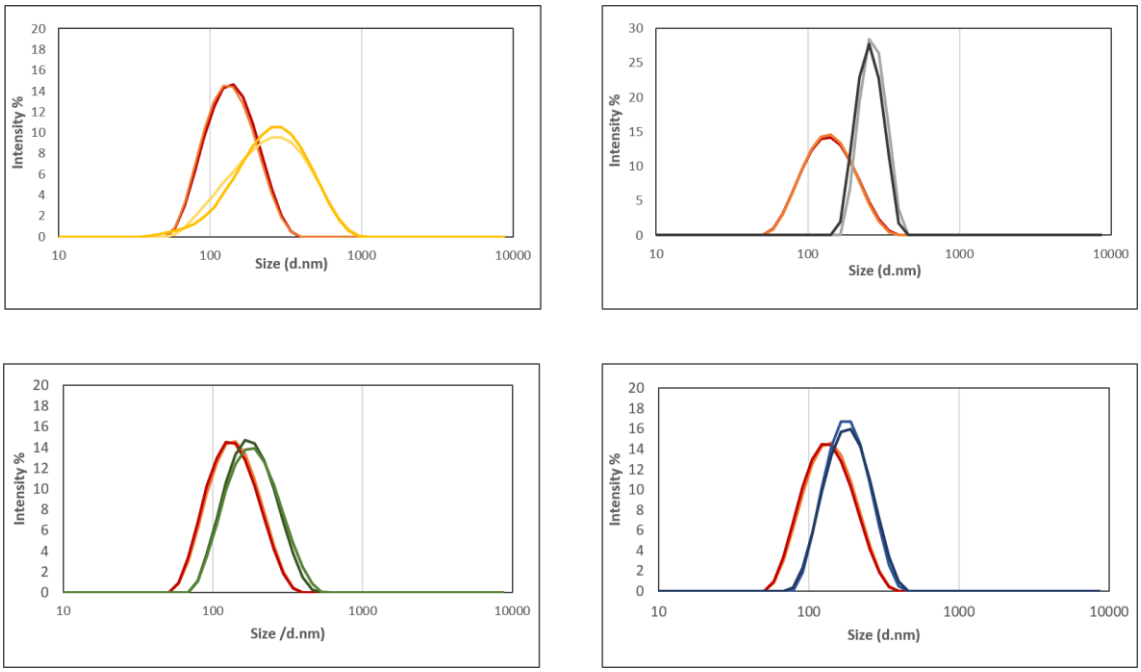

Figure 9. Comparative size distribution intensity graphs of nanoparticles before and after DOX loading at studied ratios. Red: nanoparticles before loading, yellow: D/P 0.5, Grey: D/P 1, Green: D/P 2 and Blue: D/P 3.

SEM micrographs confirm that loaded particles exhibit sizes around 200 nm (Figure 10A). In addition, the images obtained by fluorescence microscopy showed bright particles at a wavelength of 561 nm characteristic of DOX emission, which confirms the drug uptake by the polymersomes (Figure 10B).

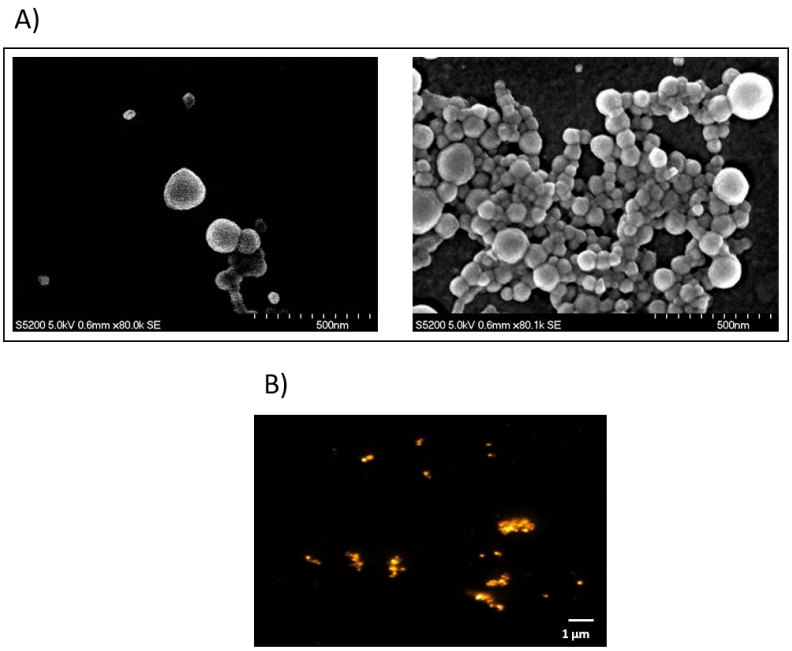

Figure 10. Microscopy images of nanoparticles loaded with DOX at DOX/polymer ratio D/P 3. A) SEM micrographs, and B) Fluorescence micrograph.

3.2.2 DOX release mediated by reduced glutathione

DOX-loaded polymersomes (DOX/polymer ratios: 0.5, 1, 2 and 3), containing disulfide bonds, behaved as smart systems that released the drug in the presence of GSH at 37 °C. DOX release from mPEG-PDH-mPEG polymersomes under these conditions showed a biphasic sustained process. It was observed a burst release within the first 10 hours for samples D/P 2 and D/P 3, followed by a more sustained release of the remaining DOX over 9 days (Figure 11). These observations indicated that the polymer chains in the polymersomes D/P 0.5 and D/P 3 were readily degraded by GSH during the first hours, providing the highest drug releases (49% and 61%) after 24 hours. In addition, both formulations presented the maximum cumulative release levels at any time, releasing about 80% of the encapsulated drug after 5 days. Formulations at DOX/polymer ratios of 1 and 2 (D/P 1 and D/P 2, respectively) released about 40% of the retained DOX, being the ones that presented the greater encapsulation efficiency.

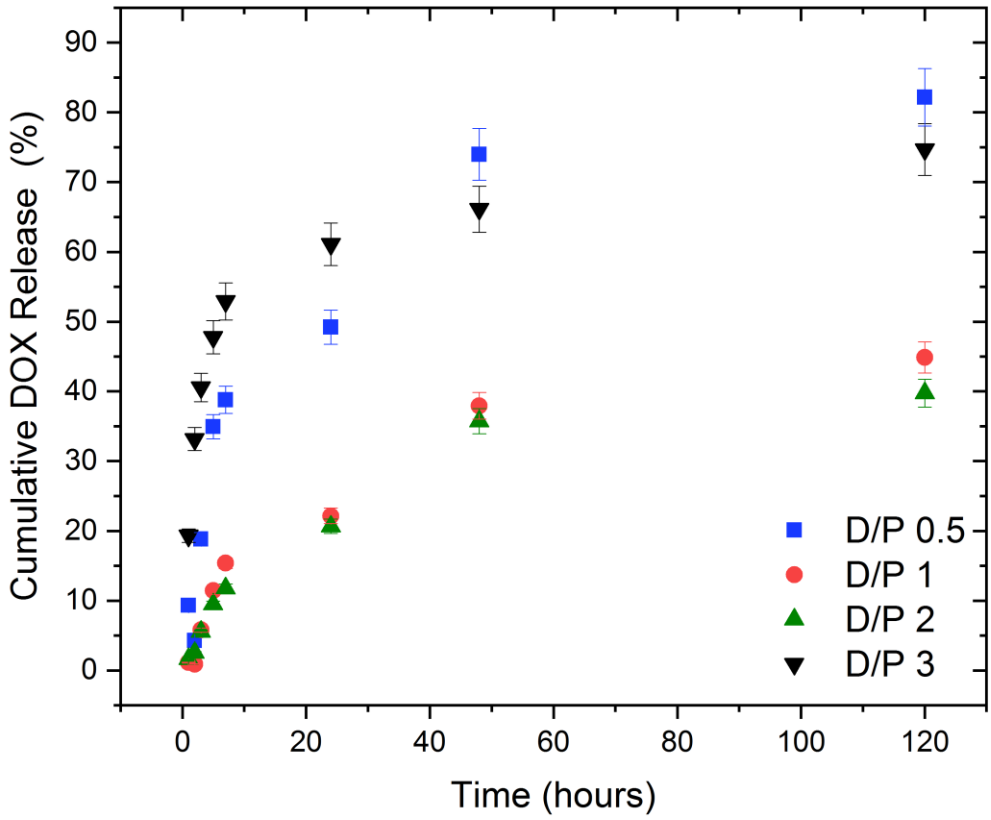

Figure 11. DOX release profiles for drug-loaded mPEG-PDH-mPEG polymersomes, at initial drug/polymer ratios D/P 0.5, D/P 1, D/P 2 and D/P 3, respectively, in the presence of GSH at 37 °C. Standard deviations are plotted with error bars in the graphs.

To demonstrate that the trigger of the drug is controlled by de presence of GSH, we carried out the drug release from D/P 1, in water at 37 ºC for 120 h. No DOX release was found during the first 10 h. After 24 h and 48 h, approximately 1% and 3.5 % DOX, respectively, were detected. Finally, around 4.5% DOX was detected after 120 h (SI, Figure S8). These results display that the release of DOX from the nanoparticles is modulated by the action of GSH.

As expected, SEM micrographs showed the state of breakage of the nanoparticles after 9 days of incubation at 37 °C in the presence of GSH. Thus, for example, Figure 12 displays the final state of the nanoparticles derived from DOX/polymer ratio 0.5 once they were degraded by glutathione. The nanoparticles had lost their structure and only amorphous clusters could be observed.

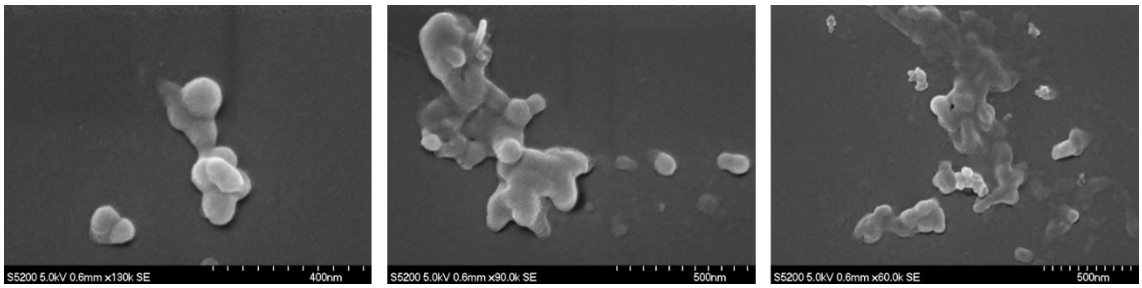

Figure 12. SEM micrographs of loaded nanoparticles of D/P 0.5 after 9 days of incubation in the presence of GSH.

4. CONCLUSIONS

In summary, in this work we report on the easy preparation of a new amphiphilic tri-*block* copolymer nominated as mPEG-PDH-mPEG, which contains multiple disulfide bonds, with potential use in drug delivery. This copolymer can self-assemble in nanometric polymersomes highly sensitive to reductive conditions. A model anticancer drug such as doxorubicin was successfully loaded in the polymersome systems with different drug/polymer ratios (D/P), and the incorporation of the drug could be verified by fluorescence microscopy. The ability of these systems to uptake and release doxorubicin was evaluated. Systems D/P 2 and 3 showed a drug loading of 62% and 69%, respectively. However, the best encapsulation efficiency was found for D/P 1 and 2, showing values close to 83%. Finally, DOX release assays were conducted at 37 °C in the presence of 0.01 M glutathione solutions. The drug was rapidly released during the first 24 hours, especially from formulations with DOX/polymer ratios 0.5 and 3, due to the reductive action of glutathione on the disulfide bonds of the polymer chains. Up to 74.6% and 82% of the encapsulated drug was released in the medium from samples D/P 3 and D/P 0.5, after 5 days of incubation. Therefore, we anticipate that the new formulated redox systems could encapsulate and control the release of other water-soluble anti-tumor drugs, presenting a high potential for pharmaceutical and biomedical applications.

Credit authorship contribution statement

Elena Benito: Conceptualization, Supervision, Investigation, Methodology, Formal analysis, Writing original draft, Writing - review & editing. **Lucía Romero-Azogil**: Investigation, Methodology, Data curation. **Elsa Galbis**: Data Curation, Formal analysis, Validation. **M.-Violante de-Paz**: Supervision, Funding acquisition, Project administration, Writing-review. **M.-Gracia García-Martín**: Conceptualization, Supervision, Funding acquisition, Project administration, Writing - review & editing.

Declaration of Competing Interest

There are no conflicts to declare.

Acknowledgments

The authors received financial support from Ministerio de Ciencia, Innovación y Universidades (MICINN) of Spain (Grants MAT2012-38044C03-01 and MAT2016-77345-C3-2-P), and Junta de Andalucía (Grant P12-FPM-1553). Lucía Romero-Azogil thanks the MICINN for a predoctoral FPI grant.

The authors thank Cristina Vaquero Aguilar (Microcopy Service, CITIUS) for the Fluorescent micrograph.

Data Availability

The raw/processed data required to reproduce these findings cannot be shared at this time due to technical or time limitations.

5. REFERENCES

[1] R.A. Smith, K.S. Andrews, D. Brooks, S.A. Fedewa, D. Manassaram-Baptiste, D. Saslow, O.W. Brawley, R.C. Wender, R. C., Cancer screening in the United States: A review of current american cancer society guidelines and current issues in cancer screening, Ca-Cancer J. Clin. 68 (2018) 297-316.
https://doi.org/10.3322/caac.21557

[2] J. Shi, P.W. Kantoff, R. Wooster, O.C. Farokhzad, Cancer nanomedicine: Progress, challenges and opportunities, Nat. Rev. Cancer. 17 (2017) 20-37. https://doi.org/10.1038/nrc.2016.108

[3] B.P. Timko, T. Dvir, D.S. Kohane, Remotely triggerable drug delivery systems, Adv. Mater. 22 (2010) 4925-4943.
https://doi.org/10.1002/adma.201002072

[4] C. von Roemeling, W. Jiang, C.K. Chan, I.L. Weissman, B.Y.S. Kim, Breaking down the barriers to precision cancer nanomedicine, Trends Biotechnol. 35 (2017) 59−171. https://doi.org/10.1016/j.tibtech.2016.07.006

[5] Z. Zhong, Innovative polymers for controlled release applications, Biomacromolecules 18 (2017) 3652−3653.
https://doi.org/10.1021/acs.biomac.7b01459

[6] N. Kamaly, B. Yameen, J. Wu, O.C. Farokhzad, Degradable Controlled-Release Polymers and Polymeric Nanoparticles: Mechanisms of Controlling Drug Release, Chem. Rev. 116 (2016) 2602−2663.
https://doi.org/10.1021/acs.chemrev.5b00346

[7] N. Li, L. Zhao, L. Qi, Z. Li, Y. Luan, Polymer assembly: Promising carriers as co-delivery systems for cancer therapy, Prog. Polym. Sci. 58 (2016) 1-26. https://doi.org/10.1016/j.progpolymsci.2015.11.002

[8] J. Nicolas, S. Mura, D. Brambilla, N. Mackiewicz, P. Couvreur, P., Design, functionalization strategies and biomedical applications of targeted biodegradable/biocompatible polymer-based nanocarriers for drug delivery, Chem. Soc. Rev. 42 (2013) 1147–1235. https://doi.org/10.1039/c2cs35265f

[9] Ch. Nehate, A.A.M. Raynold, V. Haridas, V. Koul, Comparative Assessment of Active Targeted Redox Sensitive Polymersomes Based on pPEGMA-S-S-PLA Diblock Copolymer with Marketed Nanoformulation, Biomacromolecules 19 (2018) 2549−2566. https://doi.org/10.1021/acs.biomac.8b00178

[10] Ch. Nehate, A. Nayal, V. Koul, Redox responsive polymersomes for enhanced doxorubicin delivery, ACS Biomater. Sci. Eng. 5 (2019) 70-80. https://doi.org/10.1021/acsbiomaterials.8b00238

[11] N. Casado, G. Hernández, H. Sardon, D. Mecerreyes, Current trends in redox polymers for energy and medicine, Prog. Polym. Sci. 52 (2016) 107–135. https://doi.org/10.1016/j.progpolymsci.2015.08.003

[12] H. Sun, Y. Zhang, Z. Zhong, Reduction-sensitive polymeric nanomedicines: An emerging multifunctional platform for targeted cancer therapy, Adv. Drug Delivery Rev. 132 (2018) 16−32. https://doi.org/10.1016/j.addr.2018.05.007

[13] J. Zhao, C. Yan, Z. Chen, J. Liu, H. Song, W. Wang, J. Liu, N. Yang, Y. Zhao, L. Chen, Dual-targeting nanoparticles with core-crosslinked and pH/redoxbioresponsive properties for enhanced intracellular drug delivery, J. Colloid Interface Sci. 540 (2019) 66–77.
https://doi.org/10.1016/j.jcis.2019.01.021

[14] Q. Zhang, J. He, M. Zhang, P. Ni, A polyphosphoester-conjugated camptothecin prodrug with disulfide linkage for potent reduction-triggered drug delivery, J. Mater. Chem. B. 3 (2015) 4922–4932.
https://doi.org/10.1039/c5tb00623f

[15] V. Balasubramanian, B. Herranz-Blanco, P.V. Almeida, J. Hirvonen, H.A. Santos, Multifaceted polymersome platforms: Spanning from self-assembly to drug delivery and protocells, Prog. Polym, Sci. 33(11) (2016) 1088-1118.
https://doi.org/10.1016/j.progpolymsci.2016.04.004

[16] E. Rideau, R. Dimova, P. Schwille, F.R. Wurm, K. Landfester, Liposomes and polymersomes: a comparative review towards cell mimicking, Chem. Soc. Rev. 47 (2019) 8572-8610.
https://doi.org.10.1039/c8cs00162f

[17] Y. Wang, L. Wang, B. Li, Y. Cheng, D. Zhou, X. Chen, X. Jing, Y. Huang, Compact vesicles self-assembled from binary graft copolymers with high hydrophilic fraction for potential drug/protein delivery, ACS Macro Lett. 6(11) (2017) 1186-1190.
https://doi.org/10.1021/acsmacrolett.7b00549

[18] C.G. Palivan, R. Goers, A. Najer, X.Y. Zhang, A. Car, W. Meier, Bioinspired polymers vesicles and membranes for biological and medical applications, Chem. Soc. Rev. 45(2) (2016) 377-411.
https://doi.org/10.1039/c5cs00569h

[19] T. Thambi, J.H. Park, D.S. Lee, Stimuli-responsive polymersomes for cancer therapy, Biomater. Sci. 4(1) (2016) 55-69.
https://doi.org/10.1039/c5bm00268k

[20] N. Ma, A. Song, Z. Li, Y. Luan, Redox-sensitive prodrug molecules meet graphene oxide: An efficient graphene oxide-based nanovehicle toward cancer therapy, ACS Biomater. Sci. Eng. 5 (2019) 1384−1391.
https://doi.org/10.1021/acsbiomaterials.9b00114

[21] S.V. Lale, A. Kumar, S. Prasad, A.C. Bharti, V. Koul, Folic acid and trastuzumab functionalized redox responsive polymersomes for intracellular doxorubicin delivery in breast cancer, Biomacromolecules 16 (2015) 1736−1752.
https://doi.org/10.1021/acs.biomac.5b00244

[22] Y. Shang, N. Zheng Z. Wang, Tetraphenylsilane-cored star shaped polymer micelles with pH/redox dual response and active targeting function for drug-controlled release, Biomacromolecules 20 (2019) 4602-4610.
https://doi.org/acs.biomac.9b01472

[23] A. Li, H. Ma, S. Feng, J. Liu, A copolymer capsule with a magnetic core for hydrophilic or hydrophobic drug delivery via thermo-responsive stimuli or carrier biodegradation, RSC Adv. 6 (2016) 33138-33147.
https://doi.org/10.1039/c5ra27839b

[24] H. Zhang, J. Xu, L. Xing, J. Ji, A. Yu, G. Zhai, Self-assembled micelles based on Chondroitin sulfate/poly (D,L-lactideco-glycolide) block copolymers for doxorubicin delivery, J. Colloid Interface Sci. 492 (2017) 101-111.
https://doi.org/10.1016/j.jcis.2016.12.046

[25] X. Shi, M. Hou, X. Ma, S. Bai, T. Zhang, P. Xue, X. Zhang, G. Liu, Y. Kang, Z. Xu, Starburst diblock polyprodrugs: Reduction-responsive unimolecular micelles with high drug loading and robust micellar stability for programmed delivery of anticancer drugs, Biomacromolecules 20 (2019) 1190−1202.
https://doi.org/10.1021/acs.biomac.8b01566

[26] M.V. de-Paz, F. Zamora, B. Begines, C.Ferris, J.A. Galbis, Glutathione-Mediated Biodegradable Polyurethanes Derived from L-Arabinitol, Biomacromolecules 11 (2010) 269–276.
https://doi.org/10.1021/bm9011216

[27] C. Ferris, M.V. de-Paz, A. Aguilar-de-Leyva, I. Caraballo, J.A. Galbis, Reduction-sensitive functionalized copolyurethanes for biomedical applications, Polym. Chem. 5 (2014) 2370–2381.
https://doi.org/10.1039/c3py01572f

[28] B. Begines, M.V. de-Paz, A. Alcudia, J.A. Galbis, Synthesis of Reduction Sensitive Comb-Like Polyurethanes Using Click Chemistry, J. Polym. Sci., Part A: Polym. Chem. 54 (2016) 3888–3900.
https://doi.org/10.1002/pola.28367

[29] M.D. Campinez. E. Benito, L. Romero-Azogil, A. Aguilar-de-Leyva, M.G. García-Martín, J.A. Galbis, I. Caraballo, Development and characterization of new functionalized

polyurethanes for sustained and site-specific drug release in the gastrointestinal tract, Eur. J. Phar. Sci. 100 (2017) 285–295.
https://doi.org/10.1016/j.ejps.2017.01.017

[30] L. Romero-Azogil, E. Benito, M.G. García-Martín, J.A. Galbis, Tunable hydrophilicity of redox D-mannitol-based polyurethanes modulates glutathione response, Eur. Polym. J. 94 (2017) 259–269.
https://doi.org/10.1016/j.eurpolymj.2017.07.012

[31] L. Romero-Azogil, E. Benito, A. Martínez de Ilarduya, M. G. García-Martín, Hydrolytic degradation of D-mannitol-based polyurethanes, Polym. Degr. Stab. 153 (2018) 262-271.
https://doi.org/10.1016/j.polymdegradstab.2018.05.009

[32] B. Liu, L. Tan, C. He, B. Liu, Z. Zhu, B. Gong, Y.M. Shen, Redox-responsive micelles self-assembled from multiblock copolymer for co-delivery of siRNA and hydrophobic anticancer drug, Polym. Bull. 76 (2019) 4237-4257. https://doi.org/10.1007/s00289-018-2600-y

[33] J.W. Yoo, D.J. Irvine, D.E. Discher, S. Mitragotri, Bioinspired, bioengineered and biomimetic drug delivery carriers. Nat. Rev. Drug Discovery, 10 (2011) 521−535. https://doi.org/10.1038/nrd3499

[34] D. Wu, A. Chen, C.S. Johnson Jr., An improved diffusion-ordered spectroscopy experiment incorporating bipolar-gradient pulses, J. Magn. Reson., Ser. A. 115 (1995) 260–264.
https://doi.org/10.1006/jmra.1995.1176

[35] Q.Shi, Y.B. Huang, X.S. Chen, M. Wu, J. Sun, X.B. Jing, Hemoglobin conjugated micelles based on triblock biodegradable polymers as artificial oxygen carriers, Biomaterials 30 (28) (2009) 5077-5085.
https://doi.org/10.1016/j.biomaterials.2009.05.082

[36] E. Galbis, M.V. de-Paz, N. Iglesias, B.Lacroix, A. Alcudia, J.A. Galbis, Core cross-linked nanoparticles from self.assembling polyfma-based micelles. Encapsulation of lipophilic molecules, Eur. Polym. J. 89 (2017) 406-418.
https://doi.org/10.1016/j.eurpolymj.20170.02.032

[37] L. Romero-Azogil, J.M. Benito, I. Molina Pinilla, K. Hakkou, M. Bueno Martínez, I. Cantón, P. López-Cornejo, C.B. García-Calderón, I.V. Rosado, M.-G. García-Martín, E. Benito, Structure-property relationships of D-mannitol-based cationic poly(amide triazoles) and their self-assembling complexes with DNA, Eur Polym J, 2019, 123, 109458.
https://doi.org/10.1016/j.eurpolymj.2019.109458

[38] N. Dos Santos, C. Allen, A.-M. Doppen, M. Anantha, K.A.K. Cox, R.C. Gallagher, G. Karlsson, K. Edwards, Gail Kenner, L. Samuels, M.S. Webb, M.B. Bally, Influence of poly(ethylene glycol) grafting density and polymer length on liposomes: Relating plasma circulation lifetimes to protein binding, Biochim. Biophys. Acta 1768 (2007) 1367–1377.
https://doi:10.1016/j.bbamem.2006.12.013

[39] J.S. Abramson, J.E. Amason, A.S. LaCasce, R. Redd, J.A. Barnes, L. Sokol, R. Joyce, D. Avigan, D. Neuberg, R.W. Takvorian, E.P. Hochberg, C.M. Bello, Brentuximab vedotin, doxorubicin, vinblastine, and dacarbazine for nonbulky limited-stage classical Hodgkin lymphoma, Blood 134 (2019) 606-613.
https://doi.org/10.1182/blood.2019001272

[40] O. Tacar, P. Sriamornsak, C.R. Dass, Doxorubicin: An update on anticancer molecular action, toxicity and novel drug delivery systems, J. Pharm. Pharmacol. 65 (2013) 157–170.
https://doi.org/10.1111/j.2042-7158.2012.01567.x

[41] X.B. Wang, Y.L. Jia, X.M. Su, P. Wang, K. Zhang, X. Feng, Q.H. Lui, Combination of protoporphyrin IX-mediated sonodynamic treatment with doxorubicin synergistically induced apoptotic cell death of a multidrug-resistant leukemia K562/DOX cell line, Ultrasound Med. Biol. 41 (2015) 2731-2739.
https://doi.org/10.1016/j.ultrasmedbio.2015.06.001

[42] N. Iglesias, E. Galbis, M.J. Díaz-Blanco, M.V. de-Paz, J.A. Galbis, Loading studies of the anticancer drug camptothecin into dual stimuli-sensitive nanoparticles. Stability scrutiny, Int. J. Pharm. 550 (2018) 429–438.
https://doi.org/10.1016/j.ijpharm.2018.08.026

[43] L. Dai, Ch.-X. Li, K.-F. Liu, H.-J. Su, B-Q. Chen, G.-F. Zhang, J. He, J.-D. Lei, Self-assembled serum albumin–poly(L-lactic acid) nanoparticles: a novel nanoparticle platform for drug delivery in cancer, RSC Adv. 5 (2015) 15612-15620.
https://doi.org/10.1039/c4ra16346j